21st Australasian Fluid Mechanics Conference
Adelaide, Australia
10-13 December 2018

Examination of the Details of 2D Vorticity Generation Around the Airfoil During Starting and Stopping Phases

Alwin R. Wang and Hugh M. Blackburn

Department of Mechanical and Aerospace Engineering
Monash University, Victoria 3800, Australia

Abstract

This paper presents a numerical study of vorticity generation around a 2D airfoil during the starting and stopping phases of motion. The study focuses on a single NACA0012 airfoil of unit chord at 4° angle of attack where the two-dimensional Navier-Stokes equations are solved using a spectral element DNS code. TO COMPLETE

Introduction

Around 1930 Prandtl, Tietjens and Müller recorded the motion of fine particles around an airfoil in the starting and stopping phases of motion to observe transient, unsteady flows[9]. The original recordings have been analysed using modern particle image velocimetry (PIV) by Willert and Kompenhans [14] and the phenomena of starting and stopping vortices still remains of interest.

<IMAGE from Willert>

Vincent and Blackburn [12] showed the formation of these vorticies by performing a direct numerical simulation (DNS) of transient flow over a NACA0012 airfoil at $\mathrm{Re} = 10,000$ and $\alpha = 4°$ while Agromayo, Rúa and Kristoffersen [1] investigated a NACA4612 at $\mathrm{Re} = 1,000$ and $\alpha = 16°$ using OpenFOAM. Both studies determined coefficients of lift and drag during the starting and stopping phases and verified Kelvin's and Stoke's theorems, shown in equation (1), for vorticity around various contours. This paper extends on these studies by considering the vorticity generation mechanisms and exploring the physical phenomina behind leading edge vortices observed during the stopping phase.

$$\Gamma = \oint_C \vec{V}\cdot \mathrm{d}\vec{l} = \iint_S \vec{\nabla}\times\vec{v}\cdot \mathrm{d}S = \iint_S \vec{\omega}\cdot \mathrm{d}\vec{S} \tag{1}$$

It is recognised that the sources of vorticity must occur at the boundary of the fluid regions and for the starting and starting and stopping phases of motion. Morton [10] outlines two production mechanisms for vorticity: tangential pressure gradients from the fluid side, and the acceleration of the surface from the wall side, shown in equation (2). These contributions were investigated by Blackburn and Henderson [3] for vortex shedding of oscillating cylinders and it was noted that the pressure-gradient generation mechanism could override the surface-acceleration generation mechanism and vice verse.

$$-\nu\left(\frac{\partial\vec{\omega}}{\partial z}\right)_0 = -\frac{1}{\rho}\left[\left(\vec{n}\times\nabla\right)\vec{p}\right]_0 - \vec{n}\times\frac{\mathrm{d}V}{\mathrm{d}t} \tag{2}$$

Zhu et al. [15] investigated the casual mechanisms for airfoil circulation using vorticity creation theory based on Lighthill's relations [6], shown in equation (3), instead of boundary-layer theory. Additionally, the realisation of the Kutta condition and creation of starting vortex was determined to be through a complex chain of processes which were also explained by considering boundary vorticity flux, σ, also shown in equation (3).

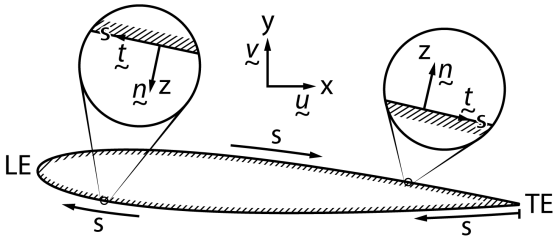

Figure 1: Coordinate system used

$$\frac{1}{\rho} = \frac{\partial p}{\partial s} = \nu\frac{\partial\omega}{\partial n} \equiv \sigma \tag{3}$$

Another phenomena of interest identified by Vincent and Blackburn [12] and Agromayo, Rúa and Kristoffersen [1] was the large value of lift during the starting (accelerating) phase. The explanation can be attributed to unsteady flows over airfoils given by Kármán and Sears [5] and later extended by Liu et al. [8] and Limacher, Morton and Wood [7]. After the starting phase when the airfoil had attained a uniform velocity, it was also observed the lift force would asymptote to a steady-state value. An explanation given by Kármán and Sears [5] was due to a "lift deficiency" term due to the wake vorticity sheet generated during acceleration. This behaviour was also detailed in Saffman explaining latency in lift production known as the "Wagner effect" [11, 13].

Both of these effects will also be investigated when the vorticity is not contained to a thin region as is the case here due to the low Reynolds number and from a vorticity production perspective.

Numerical Method

Governing Equations and Numerical Approach

Simulation was carried out using the Semtex code [4] which is a spectral element-Fourier DNS code. The governing equations solved were the non-dimensionalised Navier-Stokes equations in the moving reference frame fixed to the airfoil,

$$\nabla\cdot\vec{u} = 0 \tag{4}$$

$$\frac{\partial\vec{u}}{\partial t} + \vec{u}\cdot\nabla\vec{u} = -\nabla\vec{P} + \frac{1}{\mathrm{Re}}\nabla^2\vec{u} - a \tag{5}$$

where $\vec{P} = \frac{\vec{p}}{\rho}$ and a is the acceleration of the reference frame. The boundary conditions at prescribed-velocity boundaries are set as $u = -V(t)$ where $V(t)$ is the velocity of the reference frame such that $a = V'(t)$.

For motion of a two-dimensional plane boundary moving in its own plane with velocity $V = (V(t), 0)$, the diffusive flux density (flow per unit lenth per unit time) of positive vorticity outwards from the wall is given as

$$-\sigma \equiv -\nu\frac{\partial\vec{\omega}}{\partial z}\Big|_{z=0} = -\vec{n}\times\left(\nabla\vec{P} + \vec{a}\right) \tag{6}$$

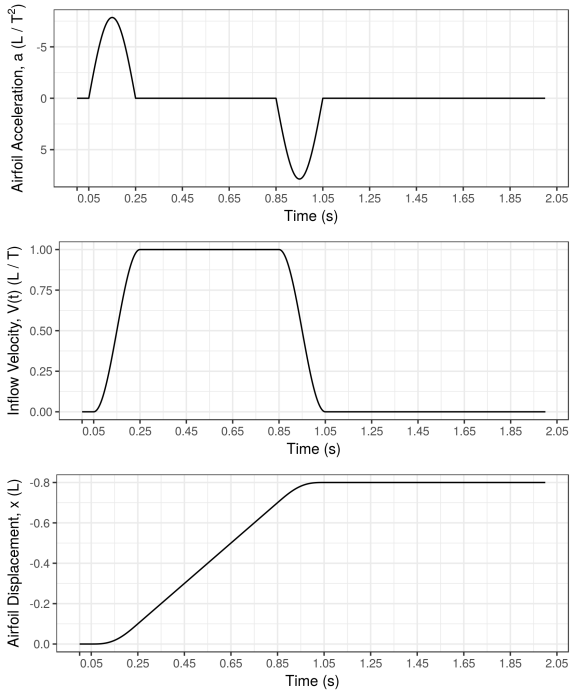

Figure 2: Airfoil during the starting and stopping phases. Note that the definition of x is consistent with the solution domain the accelerating reference frame.

where $\vec{\omega}$ is the vorticity, $\vec{n}$ is the unit wall-normal vector, z is the distance normal to the surface and $\vec{a}$ is the local wall acceleration [10]. The term boundary vorticity flux (BVF), σ, has been introduced based on Zhu et al. [15].

It is assumed that a local section of airfoil can be modelled as an infinite plane with negligible curvature and the acceleration of the plane is given by $\vec{t}\cdot\vec{a}$ where $\vec{t}$ is a unit tangent vector as shown in figure 1. Thus, the vorticity production around the airfoil is given by equation 7a in vector form and equation 7b for a particular point on the airfoil.

$$-\nu\vec{n}\cdot\nabla\vec{\omega} = -\vec{n}\times\nabla\vec{P} - \vec{t}\cdot\vec{a} \tag{7a}$$

$$-\nu\frac{\partial\omega}{\partial z} = -\frac{1}{\rho}\frac{\partial p}{\partial s} - \frac{\mathrm{d}V}{\mathrm{d}t} \tag{7b}$$

It is clear that the convergence of second derivatives for u and v will be required to accurately determine $\nabla\vec{\omega}$.

The acceleration profile for the airfoil was chosen to be the same as Vincent and Blackburn [12] which represents non-impulsively started flow to unity free-stream velocity (figure 2). In Saffman's detail of the [11] explaining the "Wagner effect" [13], it is noted that the initial lift is one-half of the final steady-state lift after a time $O(c/v)$. As such, a period of 0.8 s of uniform flow between the starting and stopping phases allows the convergence of lift to be investigated without the need for an excessively long grid domain to prevent the starting vortex "leaving" the solution domain in the reference frame of the airfoil.

Grid and Time Step Refinement

Additional refinement on the mesh used by Vincent and Blackburn [12] was performed to obtain convergence of second derivatives. The local mesh density at the leading edge and trailing edge were increased and the order of the tensor product nodal basis functions. Figure 3 shows the benefit on the second derivatives for increasing the mesh density and order.

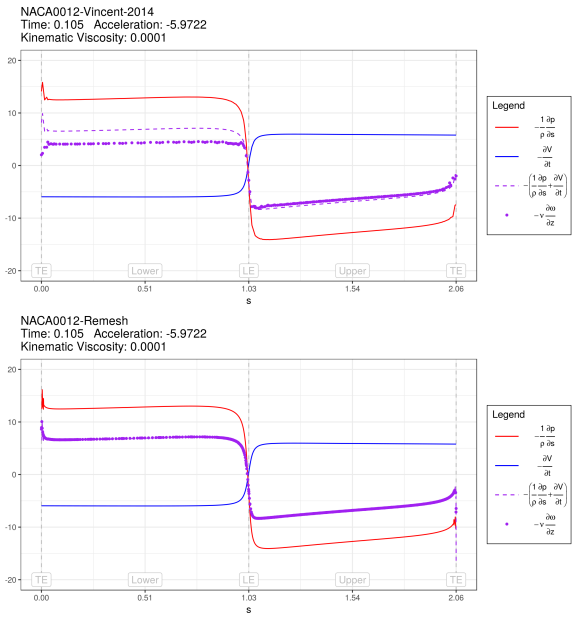

Figure 3: Comparison in ability to resolve equation (7b) for vorticity generation. The dashed purple line represents the RHS of the equation and the purple dots represent the LHS.
Top: Vincent and Blackburn [12] mesh, $p = 5$.
Bottom: Refined mesh, $p = 8$.

To determine an appropriate choice for the order of the tensor-product GLL shape functions used in each spectral element, tests were conducted at $t = 0.15\,\mathrm{s}$ which corresponded to the maximum forwards (negative) acceleration of the airfoil.

The final spectral element mesh used had X conforming quadrilateral spectral elements as shown in Y. Local mesh refinement was concentrated near the surface of the airfoil to resolve the boundary layer. X-order tensor-product nodal basis functions were used in each element, giving a total of X independent mesh nodes.

Unsteady Thin-Airfoil Theory

According to classic thin airfoil theory provided in Anderson [2] the vortex sheet strength of an airfoil, $\gamma(\xi)$, can be determined as

$$\frac{1}{2\pi}\int_{-1}^{1}\frac{\gamma(\xi)}{x-\xi} = V_\infty\left(\alpha - \frac{\mathrm{d}z}{\mathrm{d}x}\right) \tag{8}$$

where the terminals have been adjusted to match the definition provided in [5] and $\frac{\mathrm{d}z}{\mathrm{d}x} = 0$ in this analysis as the NACA0012 is a symmetric airfoil. The transformations $\xi = -\cos(\theta)$ and $x = -\cos(\theta_0)$ are now used to obtain the standard result

$$\gamma(\theta) = 2\alpha V_\infty\frac{1+\cos(\theta)}{\sin(\theta)} \tag{9}$$

where $\alpha = 4°$ and V_∞ is the prescribed boundary condition, $V_\infty = -V(t)$, for this analysis.

Kármán and Sears [5] derived the lift for an airfoil in non-uniform motion using the principles of thin airfoil theory to arrive at equation (10)

$$L = \underbrace{\rho V_\infty\Gamma_0}_{\substack{\text{Quasi-}\\\text{Steady}}} - \underbrace{\rho\frac{\mathrm{d}}{\mathrm{d}t}\int_{-1}^{1}\gamma_0(x)\,x\,\mathrm{d}x}_{\text{Apparent Mass}} - \underbrace{\rho V_\infty\int_{1}^{\infty}\gamma(\varepsilon)\frac{\mathrm{d}\varepsilon}{\sqrt{\varepsilon^2-1}}}_{\text{Wake Effect}} \tag{10}$$

where $\gamma_0(x)$ and Γ_0 are the vortex sheet strength and circulation respectively calculated from thin airfoil theory, equation (9), and $\gamma(\varepsilon)$ is the vorticity of the wake assumed to be on the airfoil plane a distance ε from the mid chord ($x = 0$). While Kármán and Sears [5] present a solution for the wake effect term, from PIV by Willert and Kompenhans [14] it is clear the assumption of the wake remaining in the same plane as the airfoil does not hold as wake vortex sheet rolls up to form the starting vortex. Thus, only the first two terms, quasi-steady state, L_0, and apparent mass, L_1, will be investigated.

Results and Discussion

Starting Vortex and Establishing the Kutta Condition

Vorticity Generation Mechanism

Unsteady Thin-Airfoil Theory

Conclusions

You should include a brief conclusion section which summarises the results of your paper.

References

[1] Agromayor, R., Rúa, J. and Kristoffersen, R., Simulation of Starting and Stopping Vortices of an Airfoil, in *Proceedings of the 58th Conference on Simulation and Modelling (SIMS 58) Reykjavik, Iceland, September 25th – 27th, 2017*, Linkoping University Electronic Press, 2017.

[2] Anderson, J., *Fundamentals of Aerodynamics*, Aeronautical and Aerospace Engineering Series, McGraw-Hill, 2010, 5 edition.

[3] Blackburn, H. M. and Henderson, R. D., A study of two-dimensional flow past an oscillating cylinder, *Journal of Fluid Mechanics*, **385**, 1999, 255–286.

[4] Blackburn, H. M. and Sherwin, S. J., Formulation of a Galerkin spectral element–Fourier method for three-dimensional incompressible flows in cylindrical geometries, *Journal of Computational Physics*, **197**, 2004, 759–778.

[5] Kármán, T. V. and Sears, W. R., Airfoil Theory for Non-Uniform Motion, *Journal of the Aeronautical Sciences*, **5**, 1938, 379–390.

[6] Lighthill, J., *An Informal Introduction to Theoretical Fluid Mechanics*, Oxford University Press, 1986.

[7] Limacher, E., Morton, C. and Wood, D., Generalized derivation of the added-mass and circulatory forces for viscous flows, *Physical Review Fluids*, **3**.

[8] Liu, T., Wang, S., Zhang, X. and He, G., Unsteady Thin-Airfoil Theory Revisited: Application of a Simple Lift Formula, *AIAA Journal*, **53**, 2015, 1492–1502.

[9] Ludwig Prandtl, O. K. G. T., *Applied hydro- and aeromechanics*, New York ; London : McGraw-Hill Book Company, inc, 1934, 1st ed edition, plates: p. [277]-306.

[10] Morton, B. R., The generation and decay of vorticity, *Geophysical & Astrophysical Fluid Dynamics*, **28**, 1984, 277–308.

[11] Saffman, P. G., *Vortex Dynamics (Cambridge Monographs on Mechanics)*, Cambridge University Press, 1993.

[12] Vincent, M. and Blackburn, H. M., Simulation of starting/stopping vortices for a lifting aerofoil, in *Proceedings of the 19th Australasian Fluid Mechanics Conference (AFMC)*, editors H. Chowdhury and F. Alam, RMIT University, 2014, 1–4, 1–4.

[13] Wagner, H., Über die Entstehung des dynamischen Auftriebes von Tragflügeln, *ZAMM - Zeitschrift für Angewandte Mathematik und Mechanik*, **5**, 1925, 17–35.

[14] Willert, C. and Kompenhans, J., PIV Analysis of Ludwig Prandtl's Historic Flow Visualization Films, *arXiv preprint*.

[15] Zhu, J. Y., Liu, T. S., Liu, L. Q., Zou, S. F. and Wu, J. Z., Causal mechanisms in airfoil-circulation formation, *Physics of Fluids*, **27**, 2015, 123601.